JOURNAL OF MATERIALS SCIENCE 33 (1998) 1639–1645

Subsurface structure of alumina associated with single-point scratching

I. ZARUDI, L. C. ZHANG*
Centre for Advanced Materials Technology, Department of Mechanical and Mechatronic Engineering, The University of Sydney, NSW 2006, Australia
D. COCKAYNE
Electron Microscope Unit, The University of Sydney, NSW 2006, Australia

The mechanisms of macroscopic ductile deformation of brittle ceramics during grinding operations are still unclear although the microcracking-free processes of grinding have been used widely in industry. This paper analyses the dislocation structure in the plastic zones of scratched alumina. It is shown that there exist three independent slip systems (two basal and one prism) and two twin systems even far below the critical onset temperatures of these systems that is usually expected. This new finding explains the formation mechanism of the macroscopic deformation induced by scratching and indicates that it is the stress field around the cutting edge which plays an important role in the activation of the slip systems. The present study offers a new insight into the mechanism understanding of material removal in ductile-regime grinding of ceramic materials. © *1998 Chapman & Hall*

1. Introduction

Crystallographic slip and mechanical twinning are the most important mechanisms of deformation in crystalline materials at temperatures up to about half the melting point [1]. Ductile behaviour of materials is associated with the possibility of changing their shape without fracture. As is well known, an arbitrary shape change is specified by six independent strain components. If a material is incompressible, the number of independent strains reduces to five. Hence, in practice the plastic deformation of a crystal must be associated with at least five independent slip or twinning systems [1]. The ductile behaviour of metals is due to the easy initiation of multiple slip systems. For ceramic crystals, however, strongly directional bonding (e.g., in covalent crystals) or electrostatic interactions (e.g., in ionic crystals) places severe restrictions on the configuration of ions at the dislocation core and therefore limits the range of slip systems. Investigations of plastic deformation of sapphire at elevated temperatures (above 1000 °C) [2–4] have identified the following slip systems: $(0\,0\,0\,1)\,\frac{1}{3}\langle 2\,\bar{1}\,\bar{1}\,0\rangle$ basal slip [2], $\{\bar{1}\,2\,\bar{1}\,0\}\,\langle 1\,0\,\bar{1}\,0\rangle$ prism plane slip [3] and $\{1\,0\,\bar{1}\,1\}\,\frac{1}{3}\,\langle 1\,\bar{1}\,0\,1\rangle$ pyramidal slip [4]. Basal slip was found to be the easiest system to be activated and pyramidal slip the most difficult [5].

The critical temperature for initiating the plastic deformation in alumina is usually considered to be 1000 °C. Nevertheless, it was found that basal and prism plane slip systems can be motivated at lower temperatures by applying a hydrostatic pressure [6–8]. Lagerlöf *et al.* [5] demonstrated that, under a hydrostatic pressure, plastic deformation in sapphire can be achieved at temperatures between $0.1\,T_M$ and $0.2\,T_M$ ($T_M = 2053$ °C is the melting point). Prism plane slip can be activated at temperatures as low as 200 °C under a hydrostatic confining pressure, and basal slip can occur at 400 °C.

Hockey and Lawn [9] showed that the plastic flow can be initiated in certain ceramics at room temperature by indentation, as a result of the high hydrostatic pressure produced in the indented zone. Their transmission electron microscopy (TEM) investigations showed a high density of dislocations and twins in several ceramics, including sapphire. Furthermore, they also found that, in alumina, mechanical polishing introduces a relatively high density of dislocations to a depth of approximately 1 μm from the polished surface [10].

The dimensions and structure of the plastic zones in alumina formed in the vicinity of the single-point scratched groove were studied by Zarudi *et al.* [11], and it was shown that plastic zones consist of high densities of dislocations and twins, although the slip systems that caused such plastic deformation were not identified.

This paper aims to investigate the slip and twin systems that cause the macroscopic plastic flow

*To whom all correspondence should be addressed.

associated with the single-point scratching of alumina, using TEM as the major technique for analysis. A theoretical method of temperature evaluation based on the principle of energy conservation is proposed to identify the temperature rise around the cutting edge.

2. Experimental details

Polycrystalline alumina specimens were made from commercially available alumina powder of 99.99% purity (Morimura Brothers Inc., Tokyo, Japan). Sintering was carried out in air at 1700 °C for 10 h. The average grain diameter of the specimen material was 25 μm. The scratching experiments were conducted on a reciprocating sliding machine, the details of which have been given in [12]. Two types of diamond indenter (a blunt conical indenter of about 100 μm tip radius and a sharp Vickers pyramid indenter with an included angle of 136°) were used to generate different contact conditions of scratching. Specimens measuring 10 mm × 6 mm × 4 mm were scratched after polishing. The normal load applied was 6 N, and the sliding speed of the indenter was 6 mm s^{-1}.

The microstructure of the subsurfaces of specimens was examined in a Philips EM 430 transmission electron microscope operating at 300 kV. To do this, a scratched specimen was first sectioned into thin slices, 1 mm thick, perpendicular to the scratched groove (Fig. 1a). Two slices were glued together in the manner shown in Fig. 1b. These were thinned mechanically and then by ion milling, to achieve a thickness of 40 nm, suitable for TEM study. If the pastic or damage zone was not fully revealed, the specimen was thinned again using the same procedure until the full area of damage could be clearly seen. This method of specimen preparation enabled the subsurface damage to be investigated thoroughly in a plane perpendicular to the scratched surface. The dislocation structure was examined using the invisibility criterion $\boldsymbol{g}\cdot\boldsymbol{b} = 0$, where $\boldsymbol{g}$ is the reflection vector and $\boldsymbol{b}$ is the Burgers vector.

Cross-sections were also examined using a Jeol 505 scanning electron microscope to reveal the dimensions of any possible damaged regions and the topography of the groove.

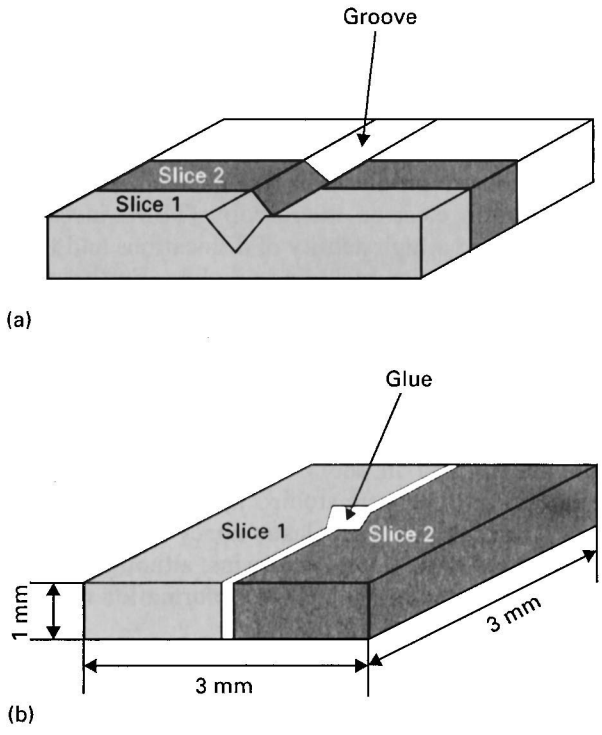

Figure 1 Preparation of specimens for TEM investigations: (a) cutting thin slices; (b) glueing two slices together.

3. Results and discussion

3.1. The initial microstructure

The structure of alumina before scratching is shown in Fig. 2. The grains were almost dislocation free.

3.2. Topography of the groove and structure of subsurface after scratching

Fig. 3a shows the topography of the groove formed by a sharp indenter. It is clear that grains are fractured and even dislodged during scratching. The damaged region is clearly seen in the scanning electron microscopy image of a cross-section perpendicular to the groove (Fig. 3b). This region is roughly hemispherical in shape with an approximate radius of 80 μm and is characterized by a high density of cracks between the grains. The structure of the material near the bottom of the groove is shown in the transmission electron micrograph in Fig. 4a. A severely deformed zone is observed, containing a high density of dislocations, deformation twins and a large number of intergranular and transgranular cracks (Fig. 4). This zone generally spreads to a depth of about two grains (20–40 μm) from the surface of the groove.

Unlike the case with the sharp indenter described above, the groove generated by the blunt indenter was very smooth, (Fig. 5a). However, this does not imply that the deformation is purely plastic, since many microcracks were formed inside the grains (i.e., trasgranular cracks) in the severely deformed layer (Fig. 5b and c).

The dislocation distribution was extremely inhomogeneous. For convenience, a region with a low

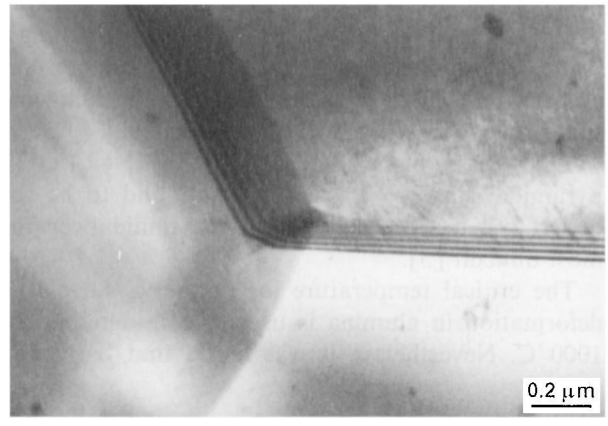

Figure 2 The initial microstructure of alumina before scratching.

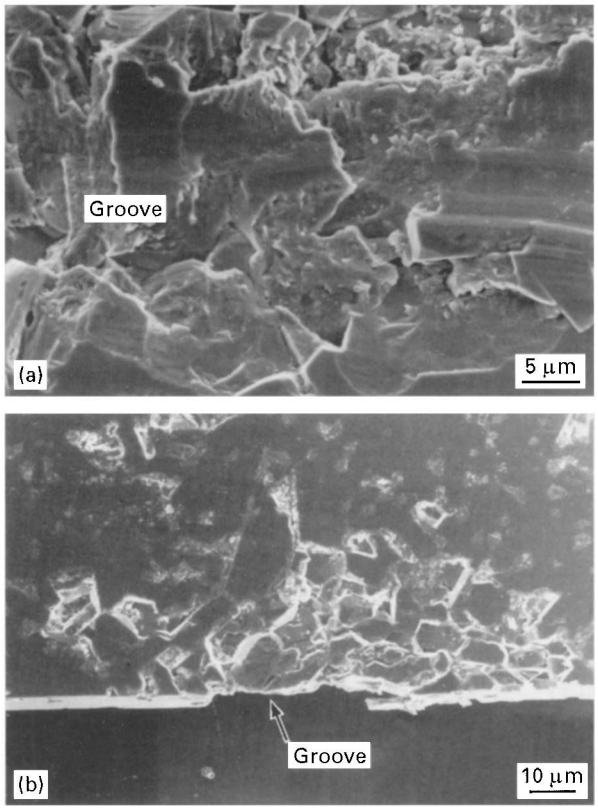

Figure 3 Alumina after scratching with a sharp indenter: (a) topography of the groove; (b) cross-section view.

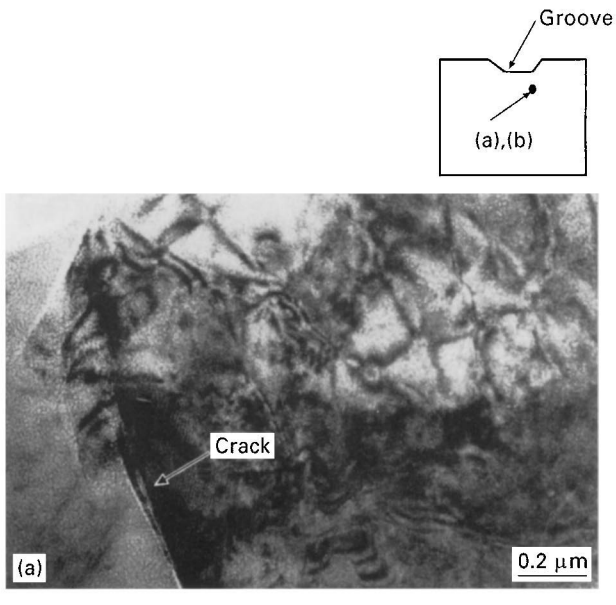

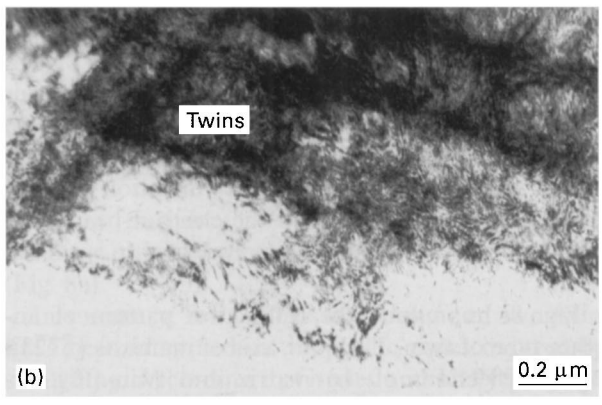

Figure 4 Structure of the plastic zone after scratching with a sharp indenter: (a) highly deformed zone under the groove with cracks; (b) dislocations and twins in the plastic zone.

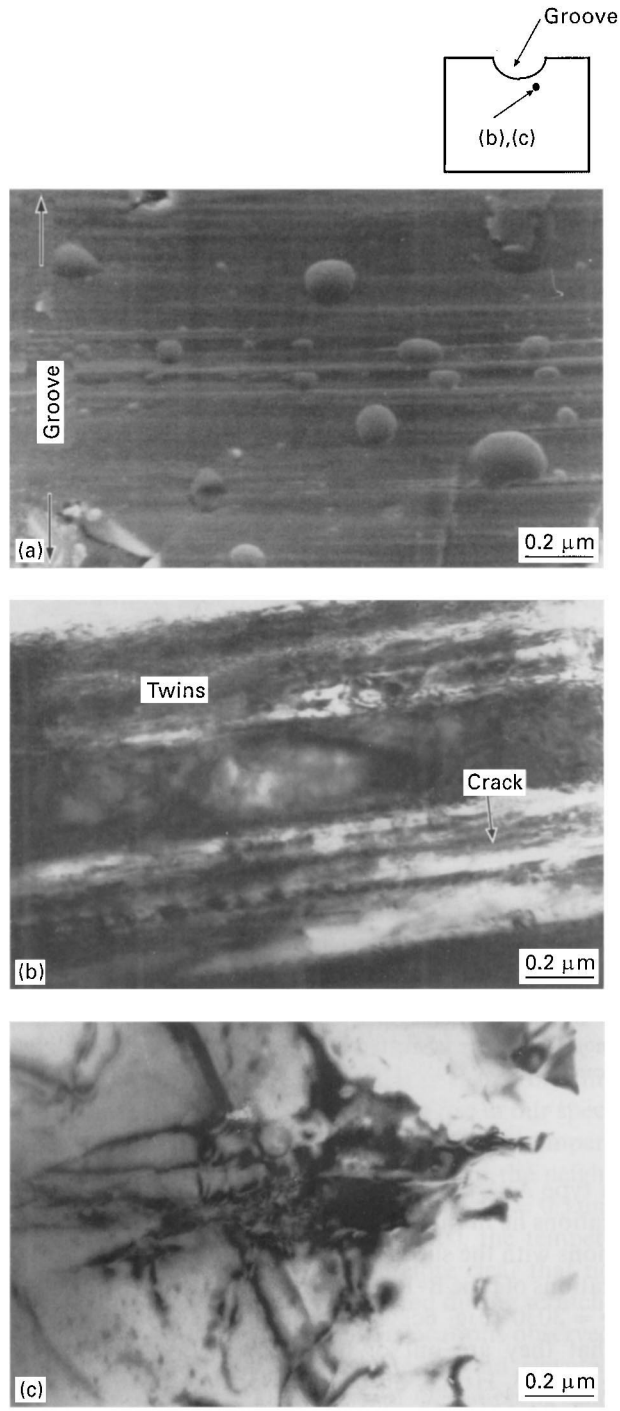

Figure 5 Alumina after scratching with a blunt indenter: (a) topography of the groove; (b) dislocation structure of the plastic zone; (c) twins in the plastic zone.

density of dislocations was chosen to resolve individual dislocations and to identify possible slip systems using TEM.

3.2.1. Basal slip system

One of the investigated regions is shown in Fig. 6. In Fig. 6a, obtained under the multiple-beam imaging conditions, a network of dislocations is shown. Fig 6b, c and d are the dark-field images of the same region obtained using the reflections $\boldsymbol{g} = \bar{3}300$, $\boldsymbol{g} = 30\bar{3}0$ and $\boldsymbol{g} = 03\bar{3}0$, respectively. The dislocations of type A–A are out of contrast in $\boldsymbol{g} = \bar{3}300$ (Fig. 6b) and $\boldsymbol{g} = \bar{3}306$. Consequently, the direction of the Burgers vector of

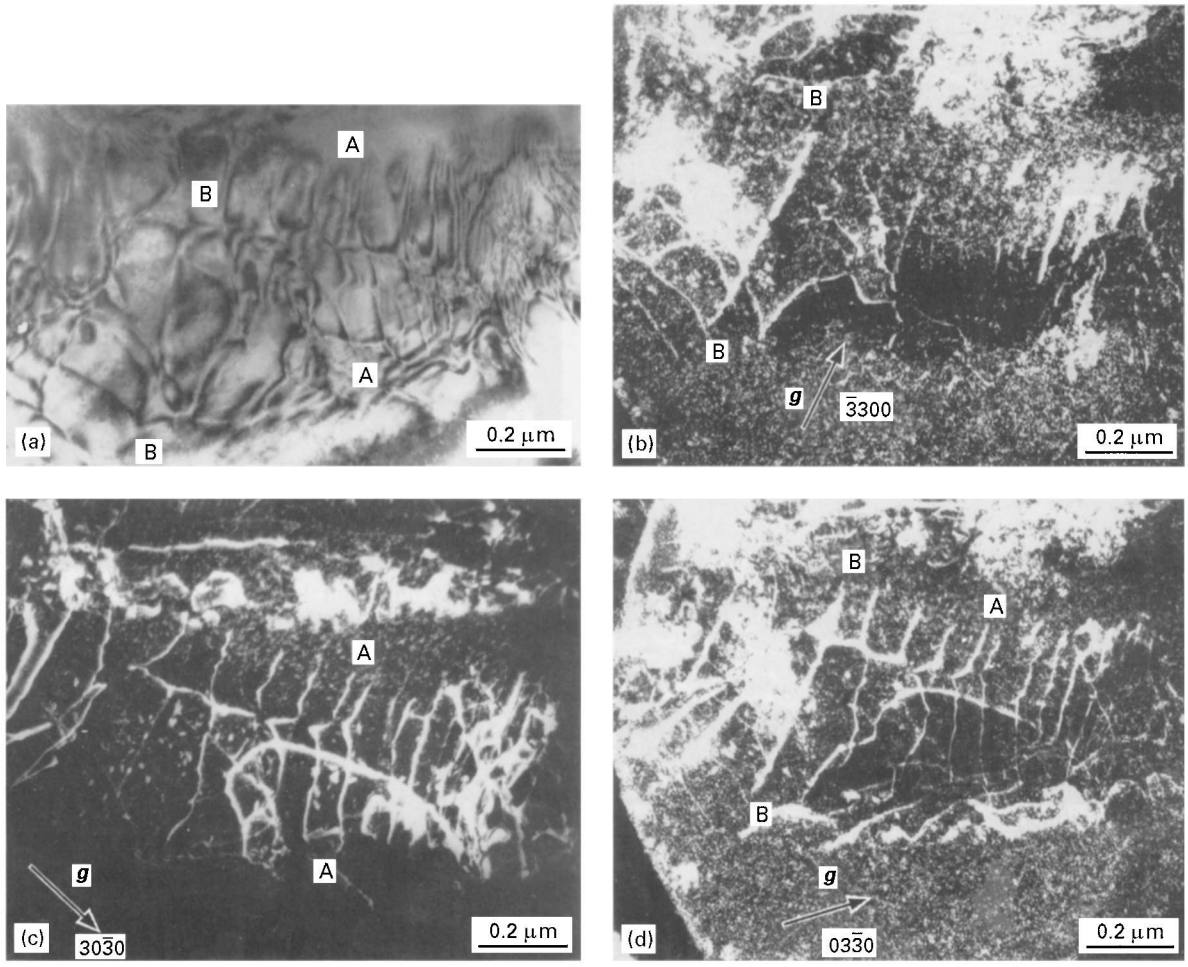

Figure 6 Basal dislocations in the plastic zone: (a) bright-field image under multiple-beam conditions (note dislocations of types A–A and B–B); (b) dark-field image in reflection $\bar{3}300$ (note that dislocations of type A–A are out of contrast); (c) dark-field image in reflection $30\bar{3}0$ (note that dislocations of type B–B are out of contrast); (d) dark-field image in reflection $03\bar{3}0$ (note that dislocations of types A–A and B–B are seen clearly).

a type A–A dislocation is $[1\,1\,\bar{2}\,0]$. Because the dislocations lie in the $(0\,0\,0\,1)$ plane, they are basal dislocations with the slip system $(0\,0\,0\,1)\,\frac{1}{3}[1\,1\,\bar{2}\,0]$. The dislocations of type B–B are out of contrast in the reflection $\boldsymbol{g} = 30\bar{3}0$ (Fig. 6c). Additional investigations proved that they are out of the contrast in the reflection $\boldsymbol{g} = 30\bar{3}3$. Hence, dislocations of type B–B are basal dislocations with a Burgers vector in the direction $[1\bar{2}10]$. The slip system is therefore deduced to be $(0001)\,\frac{1}{3}[1\bar{2}10]$.

It follows from the above study that there exist at least two different basal slip systems in alumina after scratching.

3.2.2. Prism plane slip system

A second dislocation network is shown in Fig. 7a also obtained under the multiple-beam imaging conditions. For convenience, we denote the dislocations to be analysed as type C–C and those for distinguishing the location of type C–C as type D–D. In the dark-field image with $\boldsymbol{g} = \bar{3}300$, two types of dislocation appeared. However, when using $\boldsymbol{g} = 11\bar{2}0$ and $\boldsymbol{g} = 11\bar{2}3$ in the dark-field image, the dislocations of type C–C are out of contrast (Fig. 7c). The direction of their Burgers vector is thus $[\bar{1}100]$, and the slip system is therefore a prism plane slip $\{11\bar{2}0\}\langle\bar{1}100\rangle$.

3.2.3. Deformation twins

Deformation twins were found in the plastic zone after scratching (Figs 4b and 5b). An analysis of their diffraction patterns proved that there exist two types of twin.

The diffraction pattern from the first type of twin is shown in Fig. 8b. The zone axis of the matrix is $[11\bar{2}0]$. In the diffraction pattern, reflection of the matrix and twin have been superimposed with a rotation of 180° about the axis XY. This means that the twin composition plane (K_1) is parallel to the electron beam [13]. Therefore the twin plane is (0001). Furthermore, the shear direction of the twin (η_1) is perpendicular to the electron beam, and then must be $[\bar{1}100]$. Hence this type of twin is a basal twin.

Fig. 8c represents the diffraction pattern of another type of twin. The zone axis of matrix is $[\bar{5}7\bar{2}3]$, Again reflections of the matrix and twin (Fig. 8c) are superimposed with a rotation of 180° about axis X_1Y_1. As in the previous case, this means that the direction of electron beam is parallel to the twin

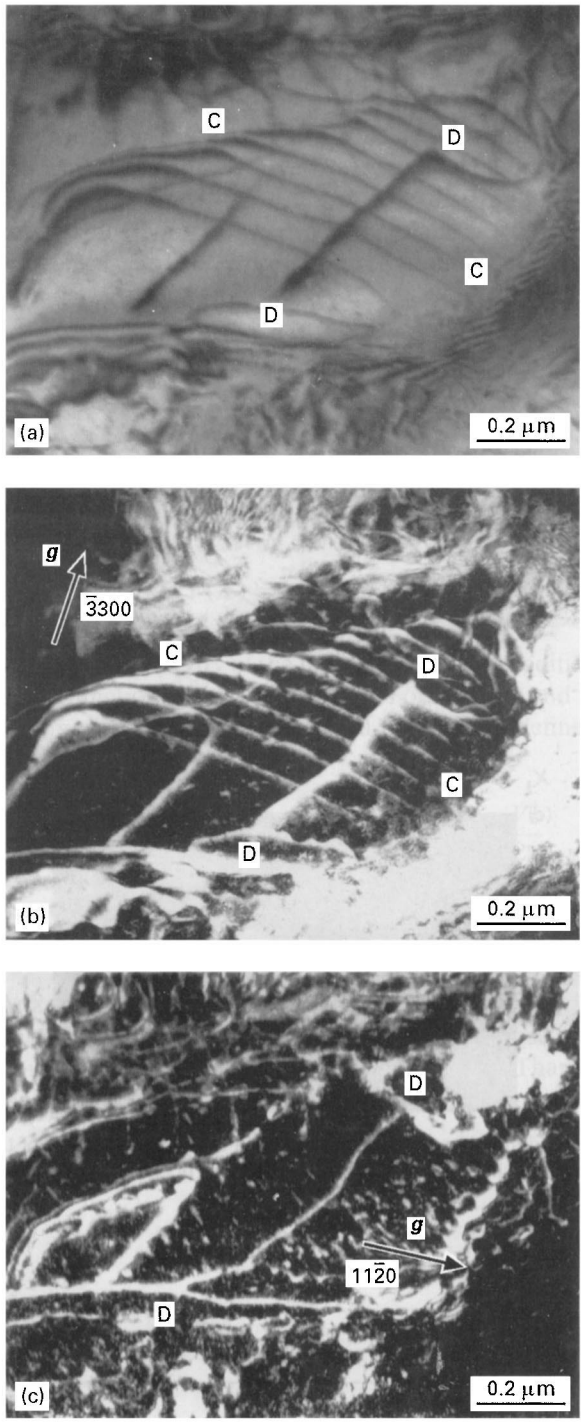

Figure 7 Prism plane dislocations in the plastic zone: (a) bright-field image under multiple-beam conditions (note dislocations of types C–C and D–D); (b) dark-field image in reflection $\bar{3}300$; (c) dark-field image in reflection $11\bar{2}0$ (note that the dislocations of type C–C are out of contrast).

plane, i.e., $K_1 = (1\,0\,\bar{1}\,1)$. Clearly it is a rhombohedral twin.

It is worthwhile to note that a crack was initiated at the intersection of the basal and rhombohedral twins (Fig. 8a).

In summary, five systems (three slip and two twin) have been identified in the plastic zones induced by scratching. According to Groves and Kelly [14] and Chin [1], they are all independent. Hence, the von Mises criterion of initiation a macroscopic plastic deformation in a polycrystalline body is satisfied.

In the following section, we discuss the mechanism giving rise to these systems.

3.3. Temperature rise during scratching

One of the possible cases of the above dislocation and twin activation is that the temperature in a zone undergoing plastic deformation rises above $0.5\,T_M$.

To examine the possible temperature rise during scratching, we apply the principle of energy conservation and assume that all the input energy through the cutting edge (the diamond indenter) was converted to heat, and that all the heat was conducted into the alumina specimen. It is clear that an analysis based on these assumptions will overestimate the temperature rise in the specimen. To examine the possible temperature rise, let us assume that the heat flux generated by scratching was distributed uniformly in a rectangular area of $-b/2 \leqslant x \leqslant b/2$ and $-b \leqslant y \leqslant b$ moving along the workpiece with a speed V, where $2b$ is the groove width and V is the speed of the diamond indenter in the scratching experiment (Fig. 9). The heat conduction problem can be solved by the Jaeger's [15] model (see Appendix A for details). (As the velocity of scratching is small ($6\,\text{mm}\,\text{s}^{-1}$), and the groove depth and the thickness of the dislocation zone are large, compared with the dimensions of an atom, this microscopic heat conduction model will give sufficiently accurate estimation of temperature rise in the workpiece.)

Using this approach, the temperature rise as a function of b is shown in Fig. 10. It is clear from this figure that the maximum temperature rise in our specimen is 20 °C, since $b = 10\,\mu\text{m}$. Moreover, the temperature rise is relatively independent of b in the neighbourhood of $b = 10\,\mu\text{m}$ and, even for $b = 0.3\,\mu\text{m}$ (which is unlikely for our experiments), the temperature rise is only 300 °C. It is therefore clear that no appreciable temperature rise occurred during scratching and that the high density of dislocations observed in the plastic zone is not activated by an elevated temperature. Hence, the cause of the slipping and twinning systems is the stress field in the vicinity of the cutting edge.

4. Conclusions

1. Five independent slip and twin systems have been found at room temperature in alumina during single-point scratching. They are two basal slip systems, $(0001)\,\frac{1}{3}[1\,1\,\bar{2}\,0]$ and $(0\,0\,0\,1)\,\frac{1}{3}[1\,\bar{2}\,1\,0]$, one prism plane slip system, $\{1\,1\,\bar{2}\,0\}\,\langle\bar{1}\,1\,0\,0\rangle$, one basal twin with $K_1 = (0\,0\,0\,1)$ and shear direction $\eta_1 = [\bar{1}\,1\,0\,0]$, and one rhombohedral twin system with $K_1 = (1\,0\,\bar{1}\,1)$ and $\eta_1 = [\bar{1}\,0\,1\,2]$.
2. These slip and twin systems make macroscopic plastic deformation possible in alumina at room temperature. The special stress field in the vicinity of the cutting edge plays an important role in the motivation of the systems.

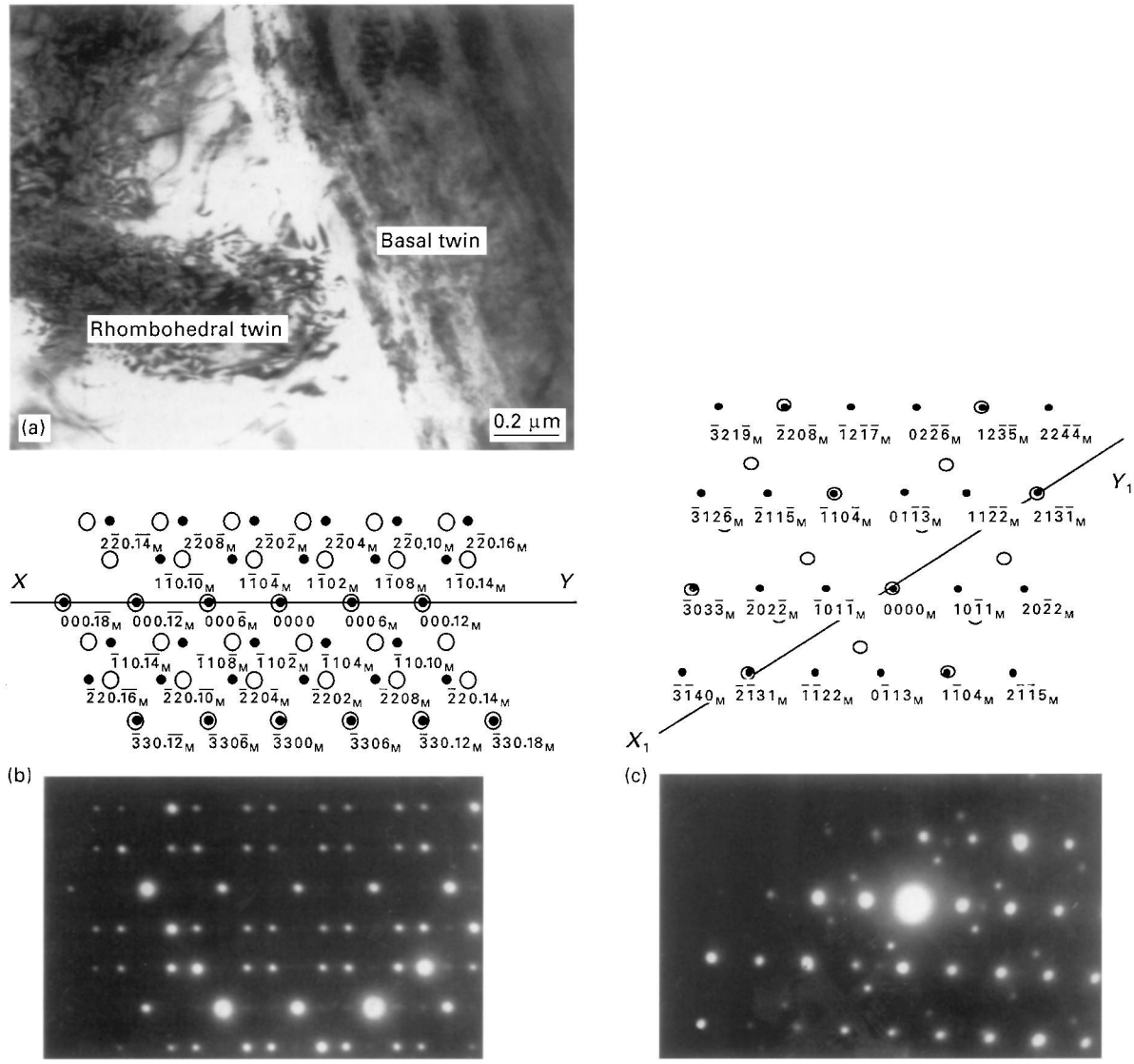

Figure 8 Twins in the plastic zone after scratching: (a) bright-field image; (b) diffraction pattern from the basal twin ((●), reflections of the matrix which are indexed; (○), reflections of twin); (c) diffraction pattern from the rhombohedral twin ((●), reflections of the matrix which are indexed; (○), reflections of twin).

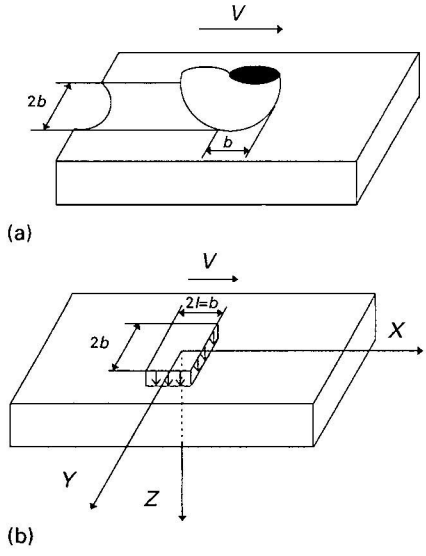

Figure 9 The model for temperature rise calculation: (a) the scratching by a diamond indenter; (b) the heat source model.

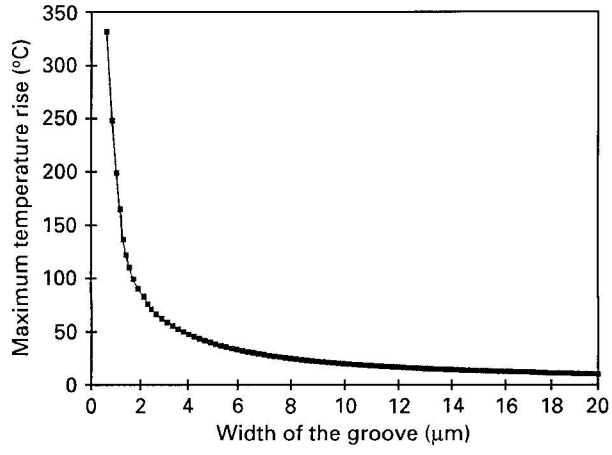

Figure 10 The maximum temperature rise in an alumina specimen during scratching.

Appendix A

The heat conduction model proposed by Jaeger [15] deals with a steady rectangular heat source, moving on the surface of a half-space along the x axis with a speed V (see Fig. 9). The heat flux, q, is uniformly distributed over a rectangular area of $-1 \leqslant x \leqslant 1$ and $-b \leqslant y \leqslant b$. The distribution of steady-state temperature rise in the plane $z = 0$ in the workpiece can be expressed in a non-dimensional form as

$$\bar{T}(X) = \int_{X-L}^{X+L} e^{-\eta} K_0(|\eta|)\, d\eta - \int_{X-L}^{X+L} e^{-\eta}\, d\eta \int_{B}^{\infty} \frac{e^{-(\eta^2+\zeta^2)1/2}}{(\eta^2+\zeta^2)^{1/2}}\, d\zeta$$

where

$$\bar{T}(X) = \frac{\pi K V}{2\varkappa q} T(X)$$

K is the conductivity of the material, k_0 is the modified Bessel function of the second kind of order zero, and $\varkappa$, X, L and B are non-dimensional parameters defined by

$$\varkappa = \frac{K}{\rho c} \qquad X = \frac{Vx}{2\varkappa} \qquad L = \frac{Vl}{2\varkappa} \qquad B = \frac{Vb}{2\varkappa}$$

where ρ is the density and c is the specific heat.

Acknowledgements

The authors wish to thank the Australian Research Council for continuing support of this project. Thanks are also due to Adam Sikorski for his help in the preparation of specimens for electron microscopy investigations.

References

1. G. Y. CHIN, in "Fracture mechanics of ceramics", edited by A. G. Evans, D. P. H. Hasselman and F. F. Lange (Plenum, New York, 1975) p. 25.
2. J. PLETKA, A H. HEUER and T. E. MITCHEL, *J. Amer. Ceram. Soc.* **57** (1974) 388.
3. J. GOOCH and G. W. GROVES, *ibid.* **55** (1972) 105.
4. J. CADOS and B. PELLSSIER, *Scripta Metall.* **10** (1976) 597.
5. K. P. D. LAGERLÖF A. H. HEUER, J. CASTING, J. P. RIVIÉRE and T. E. MITCHEL, *J. Amer. Ceram. Soc.* **77** (1994) 385.
6. J. CASTING, J. CADOZ and S. H. KIRBY, *J. Phys., Paris* **42** (1981) 43.
7. J. CADOZ, J. P. RIVIÉRE and J. CASTING, in "Deformation of ceramic materials II", edited by R. C. Bradt and R. E. Tress (Plenum, New York, 1984) p. 213.
8. J. D. SNOW and A. H. HEUER, *J. Amer. Ceram. Soc.* **56** (1973) 153.
9. B. J. HOCKEY and B. R. LAWN, *J. Mater. Sci.* **10** (1975) 1275.
10. B. J. HOCKEY, in "The science of ceramic machining and surface finishing", edited by S. J. Schneider and R. W. Rice (National Bureau of Standards, Washington, DC, 1972) p. 333.
11. I. ZARUDI, L. C. ZHANG and Y.-W. MAI, *J. Mater. Sci.* **31** (1996) 905.
12. A. K. MUKHOPADHYAY, Y.-W. MAI and S. LATHABAI, in "Ceramics", Vol. 2, edited by M. J. Bannister (Commonwealth Scientific and Industrial Research Organization, Melbourne, 1992) p. 910.
13. J. W. EDINGTON, "Practical electron microscopy in materials science", Vol 4 (Macmillan, London, 1976).
14. W. GROOVES and A. KELLY, *Phil. Mag.* **8** (1963) 877.
15. J. C. JAEGER, *Proc. Soc. NSW* **76** (1942) 204.

Received 13 May 1996
and accepted 23 October 1997